Nanoscale

PAPER

View Article Online
View Journal | View Issue

Cite this: *Nanoscale*, 2021, **13**, 939

Dendrimer–tesaglitazar conjugate induces a phenotype shift of microglia and enhances β-amyloid phagocytosis†

Louis DeRidder,[a,b] Anjali Sharma,[a] Kevin Liaw,[a,b] Rishi Sharma,[a] John John,[a,c] Sujatha Kannan[d,e] and Rangaramanujam M. Kannan[*a,b,e]

Switching microglia from a disease exacerbating, 'pro-inflammatory' state into a neuroprotective, 'anti-inflammatory' phenotype is a promising strategy for addressing multiple neurodegenerative diseases. Pro-inflammatory microglia contribute to disease progression by releasing neurotoxic substances and accelerating pathogenic protein accumulation. PPARα and PPARγ agonists have both been shown to shift microglia from a pro-inflammatory ('M1-like') to an alternatively activated ('M2-like') phenotype. Such strategies have been explored in clinical trials for neurological diseases, such as Alzheimer's and Parkinson's disease, but have likely failed due to their poor blood–brain barrier (BBB) penetration. Hydroxyl-terminated polyamidoamine dendrimers (without the attachment of any targeting ligands) have been shown to cross the impaired BBB at the site of neuroinflammation and accumulate in activated microglia. Therefore, dendrimer conjugation of a PPARα/γ dual agonist may enable targeted phenotype switching of activated microglia. Here we present the synthesis and characterization of a novel dendrimer-PPARα/γ dual agonist conjugate (D-tesaglitazar). *In vitro*, D-tesaglitazar induces an 'M1 to M2' phenotype shift, decreases secretion of reactive oxygen species, increases expression of genes for phagocytosis and enzymatic degradation of pathogenic proteins (*e.g.* β-amyloid, α-synuclein), and increases β-amyloid phagocytosis. These results support further development of D-tesaglitazar towards translation for multiple neurodegenerative diseases, especially Alzheimer's and Parkinson's Disease.

Received 14th August 2020,
Accepted 7th December 2020

DOI: 10.1039/d0nr05958g

rsc.li/nanoscale

Introduction

In the United States alone, there are currently over 5.3 million people with Alzheimer's disease (AD) and 1 million people with Parkinson's disease (PD).[1] As increased age is the largest risk factor for many neurodegenerative diseases, the prevalence and cost of treatment for these diseases will continue to increase as the population continues to grow older. Moreover, the lack of recent success in developing new drugs to treat these diseases has highlighted the need for the development of innovative therapies.[2,3] These clinical failures highlight the difficulties in developing a drug, including delivering a high enough concentration of the drug to the brain for efficacy without causing adverse side effects.

Neurodegenerative diseases such as AD and PD share three major neuropathological components: neuroinflammation, pathogenic protein accumulation, and neuronal death.[4–7] In healthy people, the innate immune cell of the brain (the microglia) constantly phagocytose the misfolded proteins (*e.g.* β-amyloid, α-synuclein) that cause neuronal death as they are produced, which prevents the hallmark aggregates from forming. However, in people who eventually develop neurodegenerative diseases, the microglia no longer remove these proteins effectively and shift into a disease exacerbating, pro-inflammatory phenotype (typically designated as M1). While the predominantly pro-inflammatory/anti-inflammatory (M1/M2) classification of microglial activation is an oversimplification of the spectrum of macrophage polarization, it is still used as a broad nomenclature to describe the dominant phenotype of microglia in neuroinflammation and in response to therapy. M1-like microglia release reactive oxygen species and other inflammatory mediators that both induce neuronal death and exacerbate disease pathology by increasing the pro-

[a]*Center for Nanomedicine, Department of Ophthalmology, Wilmer Eye Institute Johns Hopkins University School of Medicine, Baltimore, MD 21231, USA. E-mail: krangar1@jhmi.edu; Fax: +1-443-287-8635; Tel: +1-443-287-8634*
[b]*Department of Chemical and Biomolecular Engineering, Johns Hopkins University, Baltimore, MD, 21218, USA*
[c]*Department of Biomedical Engineering, Johns Hopkins University, Baltimore, 21218, USA*
[d]*Department of Anesthesiology and Critical Care Medicine, Johns Hopkins University School of Medicine, Baltimore, MD 21287, USA*
[e]*Hugo W. Moser Research Institute at Kennedy Krieger, Inc., Baltimore, MD, 21205, USA*

†Electronic supplementary information (ESI) available. See DOI: 10.1039/d0nr05958g

duction of pathogenic proteins (*e.g.* β-amyloid, α-synuclein). Moreover, the major genetic risk factors for developing AD (TREM2 and APOE) are expressed at high levels in microglia, and the TREM2/APOE pathway has been shown to cause a microglial phenotype shift in AD, amyotrophic lateral sclerosis (ALS), and multiple sclerosis animal models.[8] These findings further demonstrate the role of microglia in the pathology of multiple human neurodegenerative diseases. An approach to manipulate the phenotype of microglia would enable researchers to understand their role in neurodegenerative diseases, in addition to potentially being an effective therapeutic.

Switching microglia from a M1 to an anti-inflammatory and neuroprotective (M2) phenotype has been proposed as a therapeutic strategy to treat multiple neurodegenerative diseases.[5,6] Two currently FDA approved PPARγ agonists, type II diabetes drugs rosiglitazone and pioglitazone, have been shown to induce an M1 to M2 phenotype shift in macrophages and microglia *in vitro* and *in vivo*.[9,10] PPARγ agonists have been shown to reduce the LPS-induced secretion of reactive oxygen species by reducing the activity of NF-κB by inducing NF-κB degradation and export from the nucleus, as well as ligand-dependent transrepression.[11] Moreover, epidemiological studies have shown that diabetes patients who take rosiglitazone or pioglitazone are at a reduced risk for developing AD and PD.[12] Subsequently, rosiglitazone and pioglitazone were investigated through phase III clinical trials for AD, but failed.[13] One likely explanation for the failure of the aforementioned clinical trials is the poor transport of these drugs across the blood–brain-barrier (BBB), thus limiting the amount of drug that reached the brain of patients enrolled in these clinical trials.[14] Indeed, it is estimated that the BBB prevents about 98% of all small molecule drugs from reaching the brain, and only a fraction of the drug that enters the brain reaches the microglia.[15] In addition, PPARα is another nuclear receptor in the PPAR family.[16] It exhibits a role in lipid homeostasis and regulating inflammation, and PPARα agonists have also been shown to exhibit anti-inflammatory effects in microglia.

Clinical studies using neuroimaging, post-mortem tissue analysis, and CSF biomarkers have provided evidence that the BBB is impaired in AD and PD, as well as other neurodegenerative diseases.[17] Generation-4 hydroxyl-terminated polyamidoamine (G4-PAMAM-OH) dendrimers have been shown to intrinsically bypass the impaired BBB and accumulate in activated microglia without the need for targeting ligands, after systemic administration in multiple different neuroinflammation disease models, including in rodents, rabbits, dogs, and non-human primates.[18–28] Significantly, G4-PAMAM-OH can be administered systemically and cross the BBB in disease models with mild BBB disruption such as Rett Syndrome.[29] Additionally, the extent of uptake of G4-PAMAM-OH into the brain is directly proportional to disease severity in a rabbit model of cerebral palsy.[30] Hydroxyl terminated dendrimers have the advantage of being delivered noninvasively compared to the highly invasive, local delivery through the skull required in previous studies with other nanoparticles such as poly-ε-caprolactone and PEG, negatively charged PAMAM dendrimers, quantum dots, and nanoformulations composed of polyethylenimine (PEI) and dextran sulfate.[31–35] In addition, these hydroxyl PAMAM dendrimers are ideally positioned for translation due to their scalability and well-tolerated *in vivo* safety profile.[36–38] Due to positive pre-clinical efficacy data, a (G4-PAMAM-OH)-*N*-acetyl-cysteine conjugate is currently being evaluated in early clinical trials for childhood cerebral adrenoleukodystrophy (NCT03500627) and severe coronavirus disease 2019 (COVID-19) associated inflammation (NCT04458298).

We studied a dendrimer–drug conjugate of tesaglitazar (Tesa) attached to generation-4 hydroxyl-terminated PAMAM dendrimer. Tesaglitazar is a potent PPARα/γ dual agonist that combines the beneficial effects of PPARα and PPARγ agonists. It contains a carboxylic acid functional group for covalent conjugation to the dendrimer and for subsequent release. Additional glitazars have been developed and tested clinically, but Tesa was chosen due to its larger PPARγ to PPARα activity ratio, relatively simple chemical structure, and safety profile.[39–43] Tesa has previously reached phase III clinical trials for type 2 diabetes in the United States of America, but failed due to dose-dependent toxicity, which may be prevented by decreasing the necessary dose of administration by the controlled dendrimer delivery.[39,40,44] Since Tesa is a PPARα/γ dual agonist, its targeted delivery to activated microglia at the site of neuroinflammation could be highly beneficial. Herein, we demonstrate the synthesis and characterization of a dendrimer–tesaglitazar conjugate (D-Tesa) and demonstrate this compound's ability to induce a 'M1 to M2' phenotype shift in microglia and enhance phagocytosis of fluorescently labeled β-amyloid.

Materials and methods

Materials

1-[3-(Dimethylamino)propyl]-3-ethylcarbodiimide methiodide (EDC), 4(dimethylamino)pyridine (DMAP), $CuSO_4{\cdot}5H_2O$, sodium ascorbate, hexynoic acid and bovine serum albumin (BSA) were purchased from Sigma Aldrich US and used as received (St Louis, MO). Tesaglitazar was obtained from AstaTech Inc. (Bristol, PA). Ethylenediamine-core PAMAM dendrimer (generation 4 with 64 hydroxyl end-groups) was received from Dendritech Inc. (Midland, MI) as a solution in methanol. The dendrimer was stored in methanol at 4 °C and methanol was evaporated before use. Dialysis membrane with a molecular weight cut-off (MWCO) of 1 kDa was purchased from Spectrum Laboratories Inc. (New Brunswick, NJ). All other solvents were used as received in their anhydrous forms. All reactions, except the copper(I) catalyzed alkyne–azide cycloaddition (CuAAC) click reactions, were conducted under anhydrous conditions in organic medium with oven-dried glassware under an inert nitrogen atmosphere. For cell culture: Dulbecco's Modified Eagle Medium (DMEM), fetal bovine serum (FBS), penicillin–streptomycin (P/S), 0.05% trypsin-EDTA, and MTT reagent were obtained from Invitrogen (Carlsbad, CA, USA). Griess reagent was obtained from Promega (Madison, WI) and TNF-α ELISA was obtained from

R&D Systems (Minneapolis, MN). Analytical grade methanol was purchased from Sigma-Aldrich. Trypan blue was obtained from Corning (Manassas, VA, USA).

Synthesis procedures for D-Tesa conjugates

Tetraethylene glycol mono azide (**2**) was synthesized using a previously published protocol.[45]

Synthesis and purification of Tesa-TEG-azide (3). Tesa (950 mg, 2.32 mmol) was dissolved in 10 ml dimethylformamide (DMF). To this stirred solution, tetraethylene glycol-mono-azide (**2**, 662.1 mg, 3.02 mmol) in DMF (1 ml) was added dropwise. DMAP (255.4 mg, 2.09 mmol) and EDC (577.5 mg, 3.02 mmol) were then added to the reaction mixture, and the reaction was stirred under nitrogen purge at room temperature for 24 hours. The reaction was monitored using thin-layer chromatography and high-performance liquid chromatography (HPLC). The reaction mixture was diluted with 100 ml dichloromethane (DCM) and the crude reaction mixture was shifted into a separatory funnel, and the organic layer was subsequently washed thrice with saturated sodium bicarbonate solution, followed by saturated ammonium chloride solution and finally with brine. The organic layer was then dried with anhydrous sodium sulfate. The solvent in the organic layer was then removed using a rotary evaporator, and the solution was redissolved in 3 ml DCM and absorbed onto silica gel to be purified with a CombiFlash® chromatography system using a gradient method with ethyl acetate/hexane as the solvents to produce **3** as clear-yellow oil. The desired, pure product eluted at approximately 30–40% ethyl acetate. (Yield: 70%.)

^{1}H NMR (500 MHz, $CDCl_3$) δ 7.27 (d, J = 8.6 Hz, 2H), 7.15 (d, J = 1.9 Hz, 2H), 7.08 (d, J = 8.6 Hz, 2H), 6.73 (d, J = 8.6 Hz, 2H), 4.25–4.14 (m, 2H), 4.07 (t, J = 6.8 Hz, 2H), 3.94 (dd, J = 7.8, 5.2 Hz, 1H), 3.67–3.47 (m, 14H), 3.30 (dd, J = 8.7, 3.8 Hz, 2H), 3.06 (s, 3H), 3.02 (t, J = 6.7 Hz, 2H), 2.91–2.84 (m, 2H), 1.08 (t, J = 7.0 Hz, 3H).

ESI-MS: theoretical $C_{28}H_{39}N_3O_{10}S$: 609.24, obtained (M + 1): 610.13.

Synthesis and purification of D-YNE (5). 5-Hexyonoic acid (480 mg, 4.22 mmol) was added to a stirred solution of G4-PAMAM-OH (2.5 g, 0.176 mmol) in 20 ml anhydrous DMF. To this mixture, DMAP (430 mg, 3.52 mmol) and EDC (1 g, 5.28 mmol) were added. The reaction mixture was stirred under nitrogen purge for 24 hours at room temperature. On completion of the reaction, the reaction mixture was transferred to a 1000 MWCO dialysis tube and DMF dialysis was performed for 24 hours, and the DMF was changed about every six hours. Then dialysis with deionized (DI) water was performed for 24 hours, with the water being changed about every six hours. Lastly, the resulting dialysis tube contents were lyophilized for 48 hours, yielding a white, fluffy powder. (Yield: 61%.)

^{1}H NMR (500 MHz, DMSO) δ 8.10–7.67 (m, dendrimer internal amide H), 4.72 (s, dendrimer surface OH), 4.01 (t, ester –CH_2), 3.32 (m, dendrimer –CH_2), 3.06 (m, dendrimer and linker –CH_2), 2.85–2.58 (m, dendrimer –CH_2), 2.56–1.89 (m, dendrimer and linker –CH_2), 1.78–1.61 (m, linker –CH_2).

Synthesis and purification of D-Tesa (6). Tesa-TEG-azide (**3**, 177.8 mg, 0.303 mmol) was added to a stirred mixture of D-YNE (**5**, 350 mg, 0.023 mmol) in 5 ml of a 1 : 1 mixture of tetrahydrofuran (THF) and water with 0.5 ml of DMF in a microwave reactor safe 20 ml vial. For the CuAAC click reaction, copper sulfate pentahydrate (11.6 mg, 0.0467 mmol) and (+)-sodium-L-ascorbate (9.3 mg, 0.0467 mmol) were added to the reaction mixture. The vial was sealed, and the reaction vessel was then placed in a Biotage® Initiator microwave reactor and reacted under 20 W microwave radiation with stirring for 8 hours at 50 °C. The reaction mixture was transferred to a 1000 MWCO dialysis tube, and DMF dialysis was performed for 24 hours, with DMF being replaced by fresh solvent approximately every 4 h. Then, the contents of the dialysis tube were transferred to a falcon tube, and an equivalent amount of DI water was added. Additionally, 200 μl of ethylenediaminetetraacetic acid disodium salt solution was added to the contents of the falcon tube. This mixture was then placed into a new 1000 MWCO dialysis tube, and dialysis was performed for 12 hours in 1000 ml DI water with EDTA solution added followed by the water dialysis for 12 hours. The mixture was then lyophilized for 48 hours, and resulted in a white, fluffy powder. (Yield: 64%.)

^{1}H NMR (500 MHz, DMSO) δ 8.2–7.6 (m, dendrimer internal amide H), 7.36 (d, Tesa ArH), 7.21 (d, Tesa ArH), 7.03 (d, Tesa ArH), 6.76 (d, Tesa ArH), 4.37 (s, Tesa H), 4.18–4.04 (m, linker H), 3.96 (dd, Tesa and linker H), 3.70 (m, Tesa and linker H), 3.58–3.14 (m, dendrimer –CH_2), 3.14–2.86 (m, dendrimer –CH_2), 2.87–2.49 (m, dendrimer and linker –CH_2), 2.25 (m, dendrimer –CH_2), 1.82–1.67 (m, linker –CH_2), 0.97 (t, Tesa –CH_3).

Characterization techniques

Nuclear magnetic resonance (NMR). NMR spectra were recorded on a Bruker 500 MHz spectrometer at room temperature. Proton chemical shifts (δ) are reported in ppm. ^{1}H NMR was used to determine the number of Tesa molecules attached to each molecule of D-Tesa by proton integration method, by comparing the peaks of internal amide protons of dendrimer at δ 7.6–8.2 ppm with aromatic protons of Tesa at δ 7.36–6.76 ppm and methyl protons of Tesa in the aliphatic region.

High performance liquid chromatography (HPLC). HPLC (Waters Corporation, Milford, Massachusetts) equipped with a 1525 binary pump, an In-Line degasser AF, a 717 plus autosampler, a 2998 photodiode array detector, and a 2475 multi λ fluorescence detector interfaced with Waters Empower software was used. A Symmetry C18 reverse phase column (Tosoh, Japan) having 5 μm particle size, 25 cm length, and 4.6 mm internal diameter was used. Compounds were monitored at 210 nm and 254 nm using the PDA detectors. Solvent A was HPLC grade water with 0.1% trifluoroacetic acid (TFA), and solvent B was acetonitrile (ACN) with 5% water and 0.1% TFA. The method used started at 100 : 0 (ACN : water), decreased to 10 : 90 (water : ACN) in 5 minutes, stayed at that polarity for 15 minutes, and returned to 100 : 0 (ACN : water) in 5 minutes. The flow rate was maintained at 1 ml min^{-1}.

Mass spectroscopy. ESI-MS was performed on Bruker microTOF-II mass spectrometer using acetonitrile/water (9 : 1)

as solvent system. The molecular ions as protonated peaks $[M + nH]^{n+}$ or adducts $[M + nX]^{n+}$ (X = Na, K, or NH_4) were used to confirm empirical formula.

Dynamic light scattering and ζ-potential. A Zetasizer Nano ZS (Malvern Instrument Ltd, Worchester, U.K) equipped with a 50 mW He–Ne laser (633 nm) was utilized to determine particle size and ζ-potential distribution. D-Tesa was dissolved in DI water to a concentration of 0.2 mg ml^{-1} for DLS and in 10 mM sodium chloride to a concentration of 0.1 mg ml^{-1} for ζ-potential. The measurements were made at 25 °C, using a scattering angle of 173° as previously described.[27,46]

Drug release study. D-Tesa was dissolved at a concentration of 1 mg ml^{-1} in either phosphate buffer solution (pH 7.4) to mimic plasma conditions or sodium citrate solution (pH 5.5) to mimic lysosomal conditions. Esterases from porcine liver (from Sigma Aldrich) were added to the sodium citrate solution at the start of the release study and were replenished approximately every 3 days of the study. Each vial contained 15 ml sample and they were continuously shaken at 37 °C for the duration of the experiment. At different time points, duplicate 200 μl samples from each pH were collected and the esterase activity was subsequently quenched by adding 200 μl of methanol. Zero-hour time point samples served as the control. The samples were stored at −80 °C to further avoid any hydrolysis. The samples were further analyzed by HPLC and the area under the curve (at 210 nm) for the free drug peak was calculated. The area under the curve was correlated to the amount of drug released by utilizing a calibration curve where known concentrations of free Tesa were run on the HPLC at 210 nm.

In vitro biological assays

Cell culture. BV2 murine microglial cell line was obtained from the Children's Hospital of Michigan Cell Culture Facility. BV2 cells were cultured in Dulbecco's Modified Eagles Medium (DMEM) media with 10% heat inactivated fetal bovine serum (HI FBS) and 1% penicillin/streptomycin (P/S) at 37 °C and 5% CO_2. Once cells reached confluency in the culturing flask, the cells were passaged into a new flask utilizing 0.05% trypsin–ethylenediamine tetra-acetic acid (EDTA). For the experiments, BV2 cells were seeded in DMEM with 5% HI FBS and 1% P/S. 24–48 hours later, the cells were stimulated with 100 ng ml^{-1} (300 EU ml^{-1}) of LPS for 3 hours to allow the cells to enter a pro-inflammatory (M1) phenotype to simulate the neuroinflammatory environment present in many neurological diseases. The cells were then co-treated with LPS and either free Tesa or D-Tesa at varying concentrations for 48 h and then the supernatant and cells were collected for processing. Cells never treated with LPS (No LPS) and cells treated with LPS-only at all times (LPS-only) served as the control groups. Free Tesa and D-Tesa stock solutions were sterilized utilizing poly(ether sulfones) 0.2 μm filters. D-Tesa was soluble in the cell media. Tesa was solubilized by utilizing dimethyl sulfoxide (DMSO) at less than 0.1% (v/v) final concentration.

Cytotoxicity, nitric oxide assay, and TNF-α ELISA. For the cytotoxicity assay, cells were treated as described above in a 96-well plate, and then cytotoxicity of free Tesa and D-Tesa was assessed by MTT assay following the manufacturer's instructions. For the nitric oxide assay, cells were treated as described above in 12-well plates, and then supernatants from treated cells were collected and immediately nitric oxide levels were quantified by following the manufacturer's protocol for the Griess Reagent. For the TNF-α ELISA, cells were treated as described above in 12-well plates, and then supernatants from treated cells were collected and stored at −80 °C until ready for further processing. Then samples were thawed on ice and the TNF-α ELISA was run by following the manufacturer's protocol.

For these studies, both D-Tesa and free Tesa were sonicated and vortexed until they were both completely soluble. To solubilize free Tesa, it was first solubilized in DMSO before being diluted, where the final concentration of DMSO was under 0.1% (v/v) for all free Tesa samples. Since D-Tesa was soluble in cell culture media, DMSO was not added to those samples. For all *in vitro* studies, an equivalent amount of free or conjugated drug was applied to cells in both the free Tesa and D-Tesa groups.

Quantitative real-time PCR (qRT-PCR). Cells were treated as described above in 12-well plates, and after collecting the supernatant, cells were collected in Invitrogen™ TRIzol™ Reagent (from Fisher Scientific) and RNA was extracted by following the manufacturers protocol. The concentration and the purity of the resulting RNA was analyzed utilizing Nanodrop. Equivalent amounts of RNA from each sample was converted to cDNA by following the manufacturer's protocol for the High Capacity cDNA Reverse Transcription Kit (from Applied Biosystems by Thermo Fisher Scientific). The resulting cDNA was utilized for qRT-PCR analysis utilizing the FAST-SYBR green reagent and by following the manufacturer's protocol. Ct values were calculated by the machine and data was analyzed utilizing the $2^{-\Delta\Delta Ct}$ method. For each different marker, the ΔΔCt value was calculated by subtracting the ΔCt for the No LPS group from the ΔCt for each sample. The ΔCt value was the Ct value for the gene of interest minus the Ct for GAPDH for each given sample. Once the $2^{-\Delta\Delta Ct}$ was calculated for all groups, they were then all normalized to the No LPS group, thereby giving the No LPS group a relative expression level of 1.0 for all markers.

The forward and backward primer sequences used for qRT-PCR are shown in the below table. All sequences are written from 5′→3′.

Target	Forward sequence	Backwards sequence
TNF-α	CCA GTG TGG GAA GCT GTC TT	AAG CAA AAG AGG AGG CAA CA
IL-1β	AGC TTC AAA TCT CGC AGC AG	TGT CCT CAT CCT GGA AGG TC
IL-6	TCC AGT TGC CTT CTT GGG AC	GTG TAA TTA AGC CTC CGA CTT G
Arg1	TCATGGAAGTGAAC CCAACTCTTG	TCAGTCCCTGGCTTAT GGTTACC
IL-4	TGT AGG GCT TCC AAG GT	GAA AGA GTC TCT GCA GCT C
GAPDH	TGT CGT GGA GTC TAC TGG TGT CTT C	CGT GGT TCA CAC CCA TCA CAA

Additionally, commercially available primers were purchased from BIORAD for iNOS/Nos2 (qmmuCID0023087),

TLR4 (qmmuCID0023548), CD206/Mrc1 (qmmuCID0012670), TGF-β1 (qmmuCID0017320), IL-10 (qmmuCID0015452), SOCS1 (qmmuced0024846), CD36 (qmmucid0014852), Ide (qmmuced0049796), MMP9 (qmmucid0021296), CCL1 (qmmuced0038249), TLR8 (qmmuced0039837), CD86 (qmmucid0006086), STAT6 (qmmucid0006404), and PPARγ (qmmucid0018821).

Phagocytosis assay. The impact of free Tesa and D-Tesa on phagocytosis of β-amyloid was determined using a previously reported method.[47] Briefly, HiLyte™ Flour 488-labeled β-amyloid$_{1-42}$ (from Anaspec Inc.) was dissolved in DMSO (final DMSO concentration under 0.5% (v/v)) and diluted to 5 μg ml^{-1} in PBS. After treating the cells with Tesa and D-Tesa with the treatment scheme outlined above, the β-amyloid solution was applied to the cells for 2 hours. Then, the cells were washed thrice with Hank's Balanced Salt Solution with divalent cations (calcium and magnesium), removed from the wells using trypsin, and were resuspended in FACS buffer (from Invitrogen). Samples were stored on ice, and immediately were run on a Sony Cell Sorter SH800 flow cytometry machine, and data was analyzed with the associated software. The gate was set using cells not treated with fluorescent β-amyloid, and the results shown are the percent of cells from each group that exhibited fluorescence above the background fluorescence. The mean fluorescent intensity (MFA) of HiLyte™ 488-labeled β-amyloid was also reported for each group. This assay was performed in duplicate.

Statistics. All data shown is the result of three separate experiments, each performed in triplicate unless otherwise noted. GraphPad Prism 5 and Microsoft Excel were used to perform statistics. Two-tailed, paired Student's *t*-tests, with Bonferroni Correction, were performed. Grubbs' test was used to determine outliers. GraphPad Prism 5 for Windows was used to plot data (San Diego, CA). Data shown is the average + SEM.

Results and discussion

Synthesis and characterization of D-Tesa

To allow for targeted, intracellular delivery to activated microglial cells in the brain, Tesa was covalently conjugated on the surface of G4-PAMAM-OH with cleavable ester bonds between the drug and the dendrimer-linker (Fig. 1). In the first step, Tesa (**1**) was reacted with tetraethylene glycol azide (TEG-azide) (**2**) to produce Tesa-TEG-azide (**3**), which has an ester linkage between the drug and linker (Fig. 1A). The HPLC of compound (**3**) showed a retention time of 13.4 minutes with purity greater than 99% (Fig. S1B†). The mass spectrum of (**3**) showed a peak at 610.13 $[M + 1]^+$ corresponding to the Tesa-TEG-azide molecular weight further confirming the formation of the product (Fig. S2†). Separately, G4-PAMAM-OH dendrimer (**4**) was reacted with 5-hexynoic acid using an esterification reaction to produce D-YNE (**5**) (Fig. 1B). Lastly, Tesa-TEG-azide (**3**) and D-YNE (**5**) were reacted by the highly efficient copper-catalyzed azide–alkyne cycloaddition (CuAAC) click reaction to produce D-Tesa (**6**) (Fig. 1B).[48] The ^{1}H NMR confirmed the successful synthesis of all intermediates and the final product; D-Tesa (**6**) contained the characteristic peaks of dendrimer and drug-linker protons demonstrating the successful synthesis of D-Tesa (Fig. 2A). NMR of the final D-Tesa conjugate revealed that an average of ten molecules of Tesa were attached to each dendrimer. HPLC confirmed successful covalent conjugation, as D-Tesa exhibited a shift from both the D-YNE and Tesa-TEG-azide (Fig. 2B and S1†). Tesa has poor aqueous solubility,

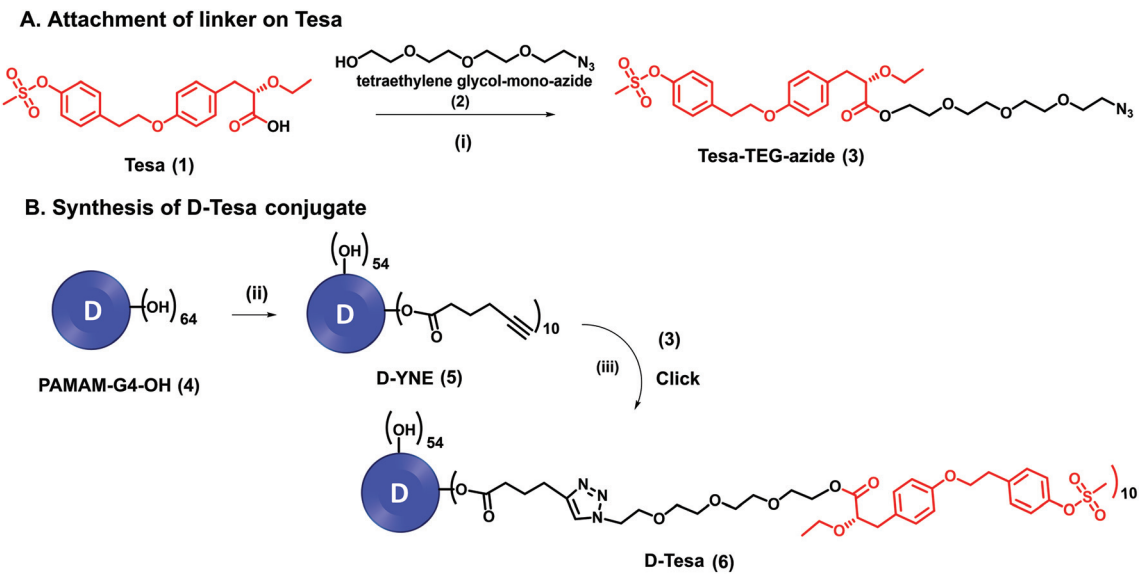

Fig. 1 Synthetic schemes for D-Tesa conjugate. (A) Synthetic route to azide-functionalized Tesa and (B) synthetic route to the conjugation of Tesa on dendrimer surface. Reagents and conditions: (i) EDC, DMAP, DMF, room temperature (rt), 24 hours; (ii) hexynoic acid, EDC, DMAP, DMF, rt, 24 hours; and (iii) CuAAC Click: Tesa-TEG-azide, $CuSO_4 \cdot 5H_2O$, sodium ascorbate, DMF, THF, H_2O, microwave, 50 °C, 8 hours.

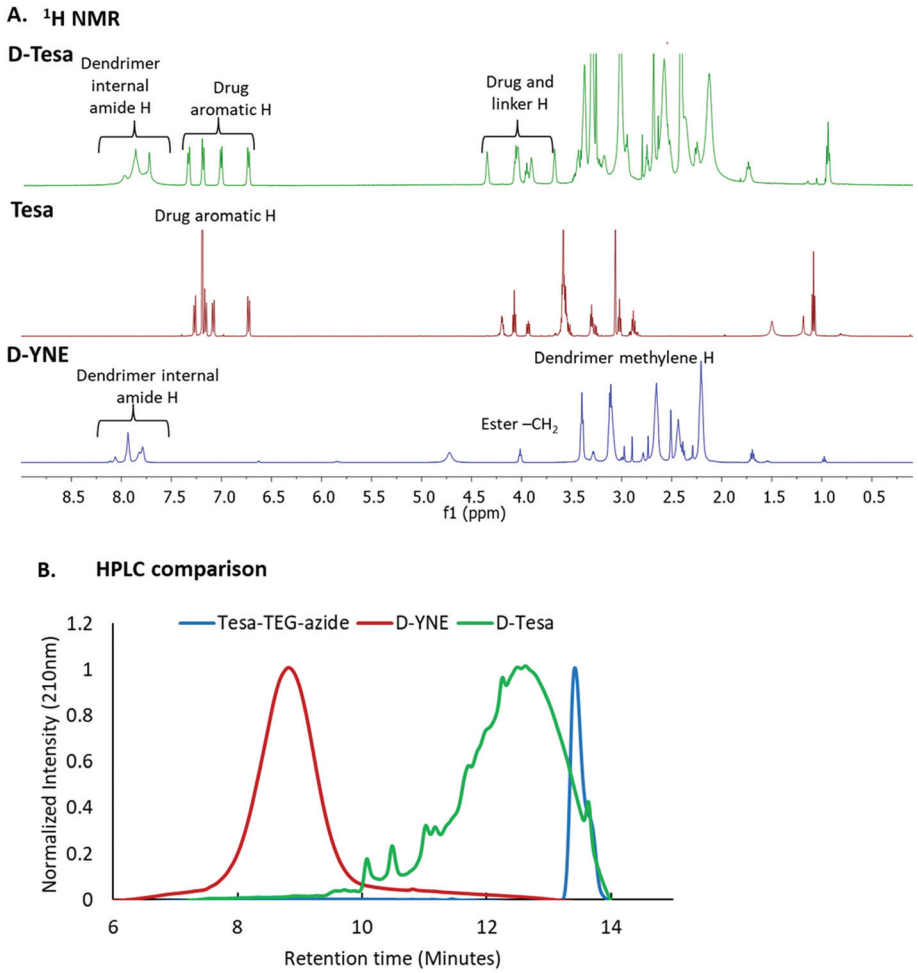

Fig. 2 Characterization of D-Tesa conjugate: (A) ^{1}H NMR showing characteristic protons of dendrimer, and drug, and (B) comparative HPLC traces of D-YNE, Tesa linker, and D-Tesa at 210 nm.

estimated to be 0.0035 mg mL^{-1}.[49] The conjugation of Tesa on hydroxyl dendrimer improved its water solubility several orders of magnitude from this estimate. D-Tesa was solubility in water at 22 mg mL^{-1}, and since Tesa comprises ~19% of the mass of D-Tesa, 4.2 mg ml^{-1} equivalent of Tesa was solubilized (Fig. 3A). The increased solubility afforded by the dendrimer increases the ease of formulation and removes the need for potentially toxic excipients.[50] These benefits are all in addition to the dendrimer's superior ability to deliver free drugs across the BBB to microglia *in vivo*, and potentially reduce the dose needed to achieve therapeutic effect.[18–28] Lastly, D-Tesa had an average size of 7.75 ± 0.29 nm (Fig. S3†), and the zeta-potential of 2.86 ± 0.38 mV (N = 5 and N = 3 measurement, respectively).

Drug release

We designed D-Tesa to release Tesa intracellularly within the low pH and high esterase concentration environment in endosomes/lysosomes of activated microglia. We have previously reported that the PAMAM dendrimers mainly enter the cells *via* fluid-phase endocytosis, and the vesicles that contain the conjugates transform into lysosomes.[51] We incubated D-Tesa at 37 °C in sodium citrate buffer (pH 5.5) in the presence of esterases to mimic the conditions of lysosomes, as performed previously.[52–54] We also investigated release under conditions that mimic plasma conditions (phosphate-buffered saline [PBS] buffer, pH 7.4). Under plasma conditions, only about 1.5% of Tesa is released after 48 hours, and less than 20% Tesa is released by day 25 suggesting the plasma stability of the conjugate (Fig. 3B). Under lysosomal conditions, about 60% of Tesa is released from D-Tesa within the first 48 hours, and within 19 days, nearly 100% of Tesa is released. These results demonstrate that D-Tesa provides sustained, triggered release of the free drug for the first two weeks incubated under physiologically relevant, lysosomal conditions. Additionally, the minimal release of Tesa in the simulated plasma conditions (pH 7.4 group) over the first 48 hours is significant, since this is the typical G4-PAMAM-OH circulation time before kidney clearance, so minimal Tesa will likely be released from the conjugates before they reach the microglia.[24]

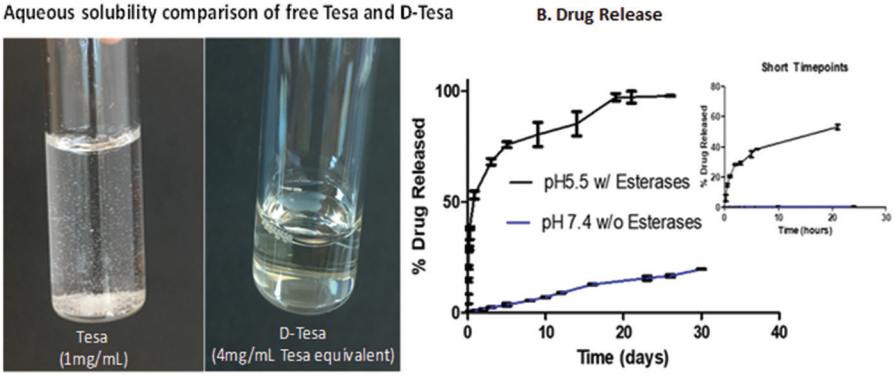

Fig. 3 Solubility and drug release study of D-Tesa. (A) Aqueous solubility comparison of free Tesa and D-Tesa. Free Tesa (1 mg mL^{-1}) is insoluble in water while dendrimer conjugated Tesa (4 mg mL^{-1}) demonstrates enhanced water solubility. (B) Drug release study to mimic drug release from D-Tesa under plasma conditions (pH 7.4, no esterases, 37 °C) and under lysosomal conditions (pH 5.5 with esterases, 37 °C). The insert allows better visualization of the drug release profile over the first twenty-four hours.

D-Tesa decreased expression of M1 markers and increased M2 markers

To evaluate the ability of D-Tesa to induce an M1 to M2 phenotype shift, we evaluated D-Tesa's ability to alter expression of M1 and M2 markers *in vitro* using a murine microglial cell line (BV2). BV2 cells were created by immortalizing murine microglial cells, and were shown to be a suitable alternative to primary microglia cells to study the microglial inflammatory response.[55,56] In our experiments, to mimic the neuroinflammatory environment present in multiple neurological diseases, we pretreated the microglia with 100 ng ml^{-1} (300 endotoxin units (EU) per ml) LPS for 3 hours. Then, we co-treated the cells with LPS and either free Tesa or D-Tesa for 48 hours, and then collected the samples. We treated the cells at concentrations of 1.5, 15, and 150 μM free Tesa or D-Tesa, on an equivalent drug basis. The MTT assay demonstrated that free Tesa or D-Tesa at these concentrations did not cause cytotoxicity (Fig. S4†). An initial dose finding study was done with Tesa and D-Tesa to determine the most effective dose of Tesa and D-Tesa. Treatment with 1.5 and 15 μM free Tesa and D-Tesa did not alter the secretion of nitric oxide or TNF-α, as determined by the Griess Reagent and a TNF-α ELISA, respectively (Fig. S5†). Based on these results, we did not analyze these lower concentrations in our qRT-PCR assays.

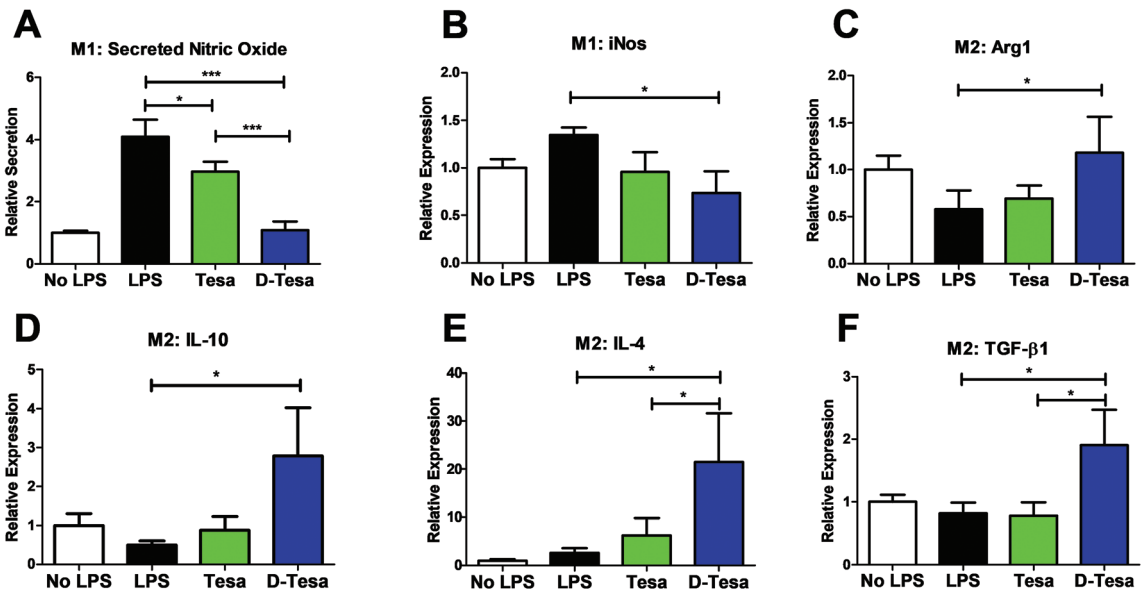

Fig. 4 D-Tesa decreases expression of M1 markers and induces upregulation of M2 markers. BV2 microglia cells were treated with LPS (100 ng ml^{-1}) for 3 hours, and then they were co-treated for 48 hours with LPS (100 ng ml^{-1}) and free tesaglitazar (Tesa) or D-Tesaglitazar (D-Tesa) at 150 μM on a drug basis. Cells that were neither treated with LPS nor drug (No LPS) and LPS only treated cells (LPS) served as the controls. (A) Supernatants were collected, and nitric oxide levels were measured using the Griess Reagent. (B–F) qRT-PCR analysis of the M1 marker: (B) iNOS, and the M2 markers: (C) Arg1, (D) IL-10, (E) IL-4, and (F) TGF-β1. All data is mean + SEM ($N = 3$). *$p < 0.05$, ***$p < 0.001$ (Bonferroni corrected).

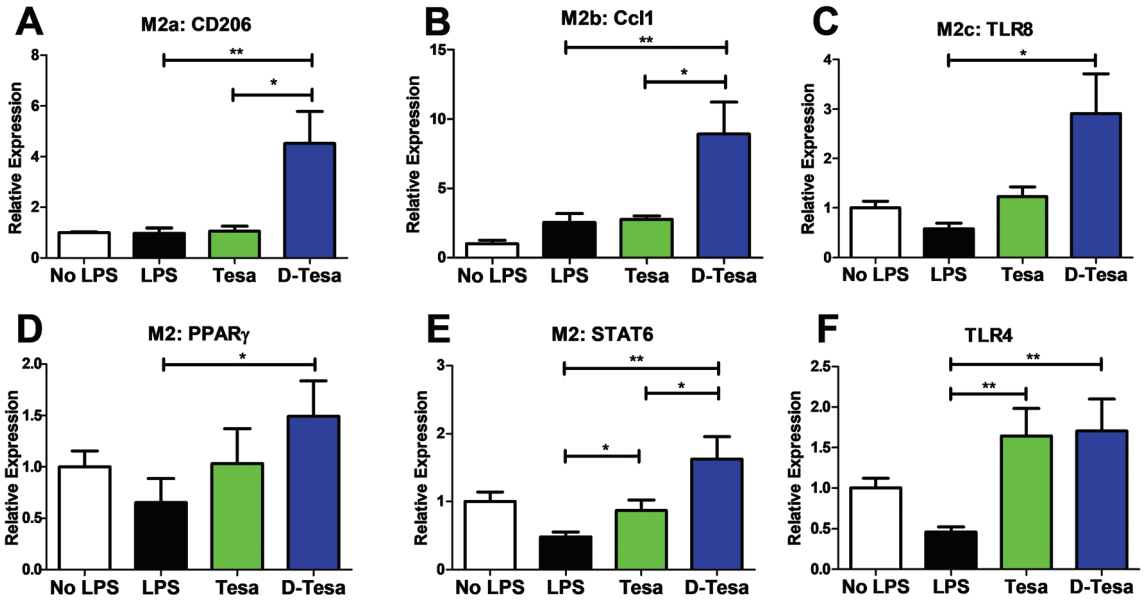

Fig. 5 D-Tesa induces a M2-mixed phenotype in microglia and modulates expression of key proteins in the IL-4/STAT6/PPARγ and LPS/TLR4 pathways. BV2 microglia cells were treated with LPS (100 ng ml^{-1}) for 3 hours, and then they were co-treated for 48 hours with LPS (100 ng ml^{-1}) and free tesaglitazar (Tesa) or D-Tesaglitazar (D-Tesa) at 150 μM on a drug basis. Cells that were neither treated with LPS nor drug (No LPS) and LPS only treated cells (LPS) served as the controls. (A–F) qRT-PCR analysis of: (A) M2a marker CD206, (B) M2b marker CCl1, (C) M2c marker TLR8, (D) M2 marker PPARγ, (E) M2 marker STAT6, and (F) TLR4. All data is mean + SEM (N = 3). *p < 0.05, **p < 0.01 (Bonferroni corrected).

In many neurodegenerative diseases, one major neurotoxic function of proinflammatory, M1 microglia is their secretion of reactive oxygen species (*e.g.* nitric oxide) that directly kill neurons.[57,58] Subsequently, it has been postulated that one potential therapeutic strategy would be to decrease the secretion of these molecules. We evaluated D-Tesa's ability to achieve this effect. After LPS stimulation, D-Tesa decreased secreted nitric oxide and inducible nitric oxide synthase (iNOS) mRNA levels 3.7-fold (p < 0.0001) and 2-fold (p = 0.011), respectively, compared to cells only treated with LPS (LPS-only) (Fig. 4A and B). On the other hand, free Tesa decreased the secreted nitric oxide more moderately (1.4-fold, p = 0.004) and did not lead to a significant decrease in the iNOS mRNA expression (Fig. 4A and B). D-Tesa was much more effective than free Tesa in suppressing nitric oxide secretion. Next, depending on if microglia are in a M1 or M2 phenotype, microglia upregulate either iNOS or Arginase 1 (Arg1) to metabolize L-arginine to produce nitric oxide for their M1 pathogen killing response, or ornithine and urea for the M2 wound healing response, respectively.[59] Consistent with its downregulation of iNOS, D-Tesa increased Arg1 mRNA levels 2-fold (p = 0.011) compared to the LPS-only control, while free Tesa did not increase expression significantly (p = 0.40) (Fig. 4C). D-Tesa, and to a lesser extent free Tesa, switched microglia from releasing cytotoxic nitric oxide to metabolizing L-arginine for wound healing, which has implications in reducing, and potentially reversing, the neurotoxicity caused by microglia in neurodegeneration.[5–7,10] The downregulation of iNOS and secreted nitric oxide levels with D-Tesa treatment is in accordance with previous work that demonstrated PPARγ's natural ligand (15-deoxy-$\Delta^{12,14}$-prostaglandin J_2) decreased iNOS and nitric oxide expression and secretion in LPS treated primary microglia.[60]

IL-10, IL-4 and TGF-β1 are all cytokines that are secreted by alternatively activated M2 microglia that can induce a neuroprotective, anti-inflammatory environment in the brain.[58,61,62] Towards this end, D-Tesa increased the expression of IL-10 5.5-fold (p = 0.011) and IL-4 8.2-fold (p = 0.013) compared to the LPS-only control (Fig. 4D and E). Free Tesa did not significantly increase either IL-10 or IL-4 levels, although the averages were 1.7-fold (p = 0.066) and 2.4-fold (p = 0.11) higher, respectively, for Tesa treated microglia compared to LPS-only controls (Fig. 4D and E). Additionally, D-Tesa increased the expression of TGF-β1 2.3-fold (p = 0.015) and free Tesa did not significantly change expression (Fig. 4F). Thus, D-Tesa induces the secretion of anti-inflammatory cytokines after LPS treatment of microglia, which can mitigate the neurotoxic, pro-inflammatory environment present in neurodegenerative diseases.[5–7,10]

D-Tesa induced expression of M2-subtype markers

CD206, Ccl1, and TLR8 are specific markers for the M2a, M2b, and M2c microglia subtypes, respectively.[58] D-Tesa upregulated CD206 expression 4.5-fold (p < 0.001), Ccl1 3.5-fold (p < 0.005), and TLR8 5-fold (p < 0.01), while free Tesa did not significantly increase expression of any of these three markers (Fig. 5A–C). These data show that D-Tesa treated microglia demonstrate significant upregulation of markers of all three M2 subtypes, which agrees with the understanding that microglia phenotype is plastic and not binary.[63–65] The M1/M2 nomenclature oversimplifies the complexity that microglia can exist in a spec-

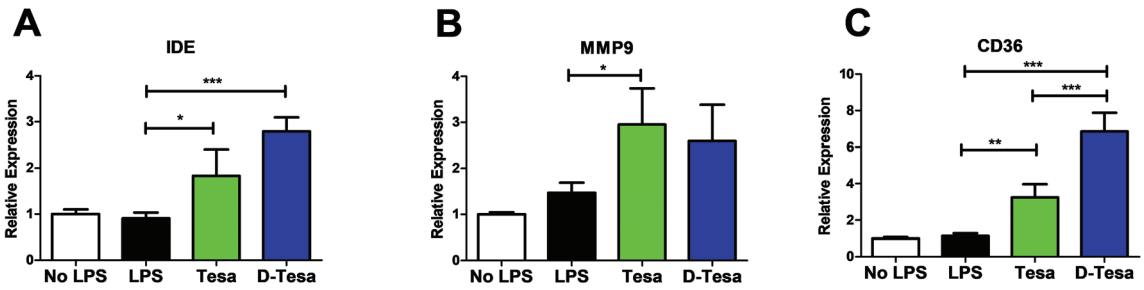

Fig. 6 D-Tesa increases expression of β-amyloid and α-synuclein degrading enzymes and scavenger receptor CD36. BV2 microglial cells were treated with LPS (100 ng ml^{-1}) for 3 hours, and then they were co-treated for 48 hours with LPS (100 ng ml^{-1}) and free tesaglitazar (Tesa) or D-Tesaglitazar (D-Tesa) at 150 μM on a drug basis. Cells that were neither treated with LPS nor drug (No LPS) and LPS-only treated cells (LPS) served as the controls. qRT-PCR analysis of: (A) insulin degrading enzyme (Ide), (B) matrix metalloproteinase 9 (MMP9), and (C) CD36. All data is mean + SEM (N = 3). *p < 0.05, **p < 0.01, ***p < 0.001 (Bonferroni corrected).

trum of activation states; along this continuum, three distinct M2 phenotypes (M2a, M2b, and M2c) have been characterized, and D-Tesa induces expression of markers consistent with each of these states.[58,61,63,66,67] M2a microglia are involved in increased phagocytosis of pathogenic proteins by upregulating scavenger receptors, tissue repair, and anti-inflammatory actions. M2b microglia are like M1 microglia in that they express IL-1β, TNF-α, and IL-6; however, M2b are distinct from M1 microglia in that they express IL-10 at high levels and downregulate iNOS expression. M2b macrophages and microglia stimulate Th2 T-cells, which is indicative of one of the roles of M2b in inducing an anti-inflammatory response. M2c microglia are involved in wound-healing, tissue remodeling, iron sequestration, and STAT3 activation that reduces pro-inflammatory signaling.[58,61,63,66]

The PPARγ activity of Tesa stimulates a feedforward loop that results in increased expression of PPARγ and its upstream signaling protein (STAT6), which are both M2a markers.[58] D-Tesa increased the expression of PPARγ 2.3-fold (p = 0.0036) and STAT6 3.4-fold (p < 0.001), while free Tesa increased STAT6 1.8-fold (p = 0.011) without a significant increase in PPARγ expression (1.58-fold increase, p = 0.17) (Fig. 5D and E). The increased expression of STAT6 and PPARγ results in anti-inflammatory gene production and inhibition of pro-inflammatory signals by inhibiting NF-κB activity. Since M2a microglia can be induced by treating microglia with IL-4, which signals through STAT6 and PPARγ, the upregulation of these two downstream signaling proteins can result in feedforward M2a polarization.[68]

In our assays, LPS activation increased IL-6, TNF-α and IL-1β levels and treatment with D-Tesa further upregulated the expression of these cytokines (Fig. S6A–D†), which is likely due to D-Tesa inducing the M2b phenotype (Fig. 5B). Free Tesa increased the expression of IL-6 and did not significantly change TNF-α and IL-1β expression (Fig. S6A–D†). While these cytokines are secreted by M1 microglia, M2b microglia also express these cytokines.[58,61] CD86 is a marker of both M1 and M2b microglia, and is increased with D-Tesa treatment (Fig. S6E†). Additionally, suppressor of cytokine signaling (SOCS) is a family of intracellular proteins that regulate the phenotypic polarization of microglia by suppressing multiple signaling pathways activated by cytokines.[69] SOCS1 is one member of this family, and it has been shown to inhibit LPS/TLR4 mediated NF-κB and JAK2 signaling, thereby reducing the amount of TNF-α, IL-1β, and IL-6 released by M1 microglia through the LPS/TLR4 pathway. D-Tesa upregulates expression of SOCS1 compared to LPS-only control (Fig. S6F†), suggesting that the increase in IL-6, TNF-α and IL-1β exhibited by D-Tesa could be due to induction of the M2b phenotype and not *via* enhancement of the LPS/TLR4, M1-inducing phenotype. Moreover, LPS signals through TLR4 and to prevent excessive cellular activation, microglia possess a negative feedback mechanism whereby TLR4 activation leads to decreased expression of TLR4.[70] Treatment with free Tesa and D-Tesa increased TLR4 levels 3.6-fold (p < 0.001) and 3.7-fold (p < 0.001), respectively (Fig. 5F), suggesting that Tesa and D-Tesa altered the typical LPS/TRL4 negative feedback signaling pathway.

D-Tesa increased expression of enzymes responsible for removal of pathogenic proteins

Insulin degrading enzyme (Ide) and matrix metalloprotease 9 (MMP9) are enzymes secreted by microglia that degrade extracellular β-amyloid and α-synuclein.[71,72] D-Tesa treatment significantly increased expression of Ide 3.1-fold (p < 0.001) with a trend towards increasing MMP9 expression (1.8-fold increase, p = 0.057) compared to LPS-only treated controls (Fig. 6A and B). Free Tesa significantly increased expression of Ide 2-fold (p = 0.011), and non-significantly increased MMP9 2-fold (p = 0.35) (Fig. 6A and B). M2 microglia in neurodegenerative diseases have the ability to remove β-amyloid, α-synuclein, and other pathogenic proteins *via* enzymatic degradation or phagocytosis, and D-Tesa upregulates proteins involved in these processes (*i.e.* Ide and MMP9).[71–73] Ide expression is downregulated in AD and PD pathology, and is known to be upregulated by PPARγ agonists, which is consistent with our results.[71,72] Functionally, only a 2-fold increase in Ide levels has been shown to decrease β-amyloid accumulation and neuronal death *in vivo*.[74,75] Therefore, the 3-fold increase in Ide observed by D-Tesa, and 2-fold increase of Ide by free Tesa could be therapeutically efficacious *in vivo*.

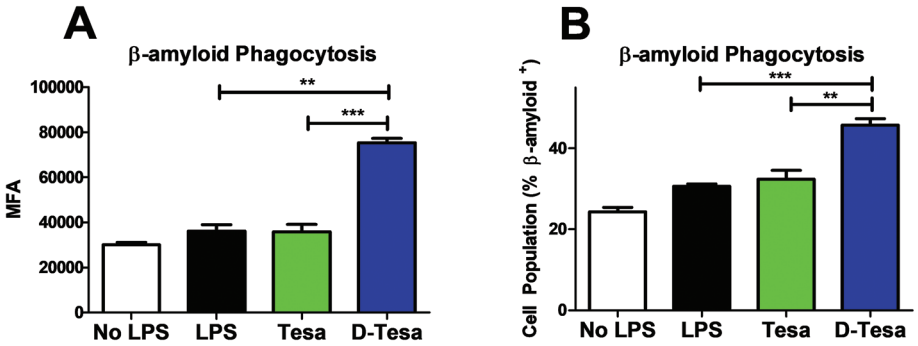

Fig. 7 D-Tesa increases phagocytosis of fluorescently labeled β-amyloid. BV2 microglia cells were treated with LPS (100 ng ml^{-1}) for 3 hours, and then they were co-treated for 48 hours with LPS (100 ng ml^{-1}) and free tesaglitazar (Tesa) or D-Tesaglitazar (D-Tesa) at 150 μM on a drug basis. Cells that were neither treated with LPS nor drug (No LPS) and LPS-only treated cells (LPS) served as the controls. Then, fluorescently labeled β-amyloid was applied to the cells for 2 hours, and cells were collected for flow cytometry. Data shown is: (A) the mean fluorescent intensity (MFA) that is proportional to amount of β-amyloid phagocytized, and (B) the percentage of cells that up took fluorescently labeled β-amyloid. All data is mean + SEM (N = 3). **p < 0.01, ***p < 0.001 (Bonferroni corrected).

D-Tesa increases phagocytosis of β-amyloid

CD36 is a microglial scavenger receptor that facilitates phagocytosis and degradation of β-amyloid.[73] Its downregulation in AD results in decreased removal of β-amyloid, but it is upregulated by PPARγ activation. Both D-Tesa and free Tesa significantly increased CD36 expression levels when compared to LPS-only exposed cells (p < 0.0001 *vs.* p < 0.005 for D-Tesa and free Tesa, respectively), but D-Tesa was much more effective than free Tesa (6-fold increase *vs.* 2.8-fold increase for D-Tesa and free Tesa, respectively, p < 0.0005) (Fig. 6C). Our results are consistent with previous studies with pioglitazone (another PPARγ agonist) that showed that increased microglial phagocytosis of β-amyloid occurs through a PPARγ and CD36 dependent mechanism.[73]

To investigate if the upregulation of CD36 from D-Tesa treatment correlated to increased phagocytic ability of these cells, we performed a functional phagocytosis assay of β-amyloid.[73] Briefly, after treating the cells as we did in the previous *in vitro* assays, we applied fluorescently-labeled β-amyloid$_{1-42}$ to the cells for two hours, washed the cells, and then performed flow-cytometry to investigate the extent of cellular uptake of β-amyloid. D-Tesa increased both the percentage of cells that phagocytosed β-amyloid and the average amount of β-amyloid internalized per cell (Fig. 7A and B). In contrast, free Tesa yielded no improvements in phagocytosis of β-amyloid. The superior effects of D-Tesa compared to Tesa is likely attributable to improved cellular internalization enabled by dendrimer conjugation. This is consistent with previous work that demonstrated over 95% of BV2 cells treated with fluorescently labeled G4-PAMAM-OH had internalized the dendrimer within thirty minutes and continued to internalize the dendrimer for at least 24 hours.[76] Likewise, conjugation of the small molecule minocycline to fluorescently-labeled G4-PAMAM-OH demonstrated 99% of BV2 cells had internalized the fluorescently-labeled dendrimer–drug conjugate within 3 hours.[26] They also showed that the conjugate reduced nitric oxide levels superior to free drug after treating BV2 cells with LPS, consistent with our results. The cells treated with D-Tesa phagocytosed 1.9-fold more β-amyloid than the LPS treated control cells (p < 0.001), which is comparable to the 2.5-fold increase of β-amyloid phagocytosis by rat primary microglial cells treated with pioglitazone reported by Yamanaka *et al.*[73] The slightly higher extent of β-amyloid phagocytosis by the previous study could be either because they did not co-treat their cells with LPS as we did, or because primary microglia express PPARγ at a higher level than BV2 cells used in this study.[77] As such, a dose of D-Tesa lower than that estimated from the *in vitro* experiments in our study can likely be efficacious in *in vivo* studies and in humans, since BV2 cells are known to express PPARγ at lower levels than primary microglia.[77]

Microglia have been implicated in many neurodegenerative diseases, and the BBB has prevented many drugs that can modify the phenotype of microglia from a pro-inflammatory, neurotoxic M1 phenotype to an anti-inflammatory, neuroprotective M2 phenotype from reaching therapeutic levels in the brain.[5,6,14,15] For example, two PPARγ agonists, pioglitazone and rosiglitazone, were each investigated through phase III clinical trials for Alzheimer's disease due to their ability to alter the phenotype of microglia, but failed likely due to poor transport across the BBB.[13,14] Thus, there is clinical interest in altering the phenotype of microglia in neurodegenerative diseases. Such an approach requires delivery of the drug to microglia at sufficient levels to drive a response. Towards this end, G4-OH-PAMAM dendrimers have been shown to deliver drugs to microglia in many animal models after systemic injection, and as a result are currently being evaluated in clinical trials for the treatment of ccALD (NCT03500627) and severe COVID-19 associated inflammation (NCT04458298).[18–28]

To combine the beneficial effects of altering microglial phenotype with the ability to deliver drugs to microglia, we conjugated tesaglitazar (a PPARα/γ dual agonist) to a G4-OH-PAMAM dendrimer (Fig. 1–3). We demonstrated that D-Tesa is capable of altering the phenotype of M1 microglia towards a M2

phenotype (Fig. 4 and 5), resulting in a decrease in secretion of harmful reactive oxygen species. Furthermore, we demonstrated that the microglia treated with D-Tesa increase their expression of enzymes that degrade pathological proteins such as α-synuclein and β-amyloid, as well as upregulating the phagocytosis of β-amyloid in a functional assay (Fig. 6 and 7). Although we do not present data demonstrating the ability of D-Tesa to bypass the BBB and accumulate in microglia, we have previously shown that G4-OH-PAMAM drug conjugates with similar drug loading, size and zeta potential are capable of passing through the impaired BBB and accumulating in microglia after intravenous administration.[26,36,52] These results support the further development of D-Tesa for the treatment of multiple neurological diseases.

While we focus on Alzheimer's and Parkinson's diseases in this paper, D-Tesa has the potential for clinical translation in multiple neurological disorders. Due to the similar role of microglia in the pathology of multiple neurodegenerative diseases, the PPARγ agonist pioglitazone was also investigated or is currently being investigated in phase II clinical trials for Parkinson's disease,[78] ALS,[79] adrenomyeloneuropathy (NCT03864523), multiple sclerosis (NCT03109288), and hematoma resolution in intracerebral hemorrhage (NCT00827892). If these clinical trials also fail due to poor delivery of pioglitazone across the BBB, D-Tesa could overcome this delivery obstacle and treat patients with these diseases.

Other groups have utilized nanoparticles to improve delivery of PPAR agonists to macrophages, but they have not attempted to deliver these agonists to microglia. Osinski *et al.* demonstrated that Tesa loaded liposomes were mostly taken up by macrophages in visceral white fat in a male leptin-deficient obesity model.[80] They additionally demonstrated that Tesa loaded liposomes did not alter the expression of the M1 marker Mcp-1, but did increase expression of the M2 marker Arg1, while treatment with free Tesa decreased the total number of M1 macrophages and expression of Mcp-1, and did not increase expression of Arg1. Nakashiro *et al.* used poly(lactic-*co*-glycolic-acid) (PLGA) nanoparticles to deliver pioglitazone (a PPARγ agonist) to macrophages in the context of atherosclerosis.[81] *In vivo*, they demonstrated that PLGA-pioglitazone reduced the levels of immune cells in the blood. In primary bone marrow derived macrophages treated with LPS and interferon-γ, they found that PLGA-pioglitazone increased IL-4 and IL-10 (M2 markers) and did not decrease IL-6 or TNF-α levels. Their findings are similar to ours; M2 markers were increased by nanoparticle-PPAR agonist treatment, while IL-6 and TNF-α levels did not decrease. Di Mascolo *et al.* used PLGA-polyvinyl alcohol nanoparticles to deliver rosiglitazone (another PPARγ agonist).[82] *In vitro* they demonstrated their nanoparticle-drug complexes decreased iNOS, TNF-α, and IL-1β expression in bone marrow derived macrophage. They pretreated their cells with the nanoparticle-drug before stimulating with LPS, while we pretreated cells with LPS before treating with D-Tesa, which could be a reason we did not observe a decrease in TNF-α and IL-1β, although we also observed a decrease in iNOS expression.

Conclusion

There is currently no pathology altering therapy for many neurodegenerative diseases, and as the population continues to age, the prevalence and cost of treating these diseases will continue to rise, highlighting the urgent need for a solution to be developed. Recently, pro-inflammatory M1 microglia have been shown to be critical in the pathology of multiple neurodegenerative diseases. Subsequently, being able to deliver a drug across the blood–brain-barrier that can induce an 'M1 to M2' phenotype shift in microglia has therapeutic potential for multiple diseases, especially Alzheimer's and Parkinson's disease. D-Tesa was designed to deliver an 'M1 to M2' inducing drug to microglia after systemic administration to reduce microglial secretion of neurotoxic substances, while also inducing an anti-inflammatory state that increases degradation and phagocytosis of pathogenic proteins in the brain. We successfully synthesized D-Tesa using a highly efficient click chemistry approach. The drug is attached to the dendrimer *via* an ester bond that is cleavable intracellularly at lysosomal conditions, with approximately 60% of Tesa being released in the first 48 hours under lysosomal conditions. D-Tesa was shown to be superior to Tesa *in vitro* in inducing an M1 to M2a/M2b/M2c phenotype shift, which resulted in reduced nitric oxide secretion, increased expression of α-synuclein and β-amyloid degrading enzymes, and increased phagocytosis of β-amyloid. Thus, D-Tesa combines the beneficial delivery properties of the dendrimer, with the M1 to M2 switching properties of Tesa. Due to the common role of microglia and the common therapeutic benefit of inducing a M1 to M2 phenotype shift, D-Tesa has the potential to treat many neurological disorders when administered at the right stage of disease progression.

Author contributions

L. D., A. S., K. L., R. S., S. K. and R. M. K. conceptualized the experiments. L. D., A. S., and R. S. performed synthesis and characterization of the dendrimer–drug conjugate. L. D., K. L., and J. J. performed the cell experiments. L. D. and K. L. performed the statistics. L. D. and A. S. wrote the manuscript, and all authors edited the manuscript.

Conflicts of interest

R. M. K. and S. K. are co-inventors of using the hydroxyl-terminated dendrimer for targeted delivery to microglia in neurological diseases, as well as patents related to the dendrimer technology described in this paper. They are co-founders of Ashvattha Therapeutics, Orpheris Inc., and RiniSight Inc., which are companies leading the clinical development of the platform. S. K. and R. M. K. are Board Members of Ashvattha Therapeutics Inc. R. S. is currently employed by Ashvattha Therapeutics and owns shares in the company; the work R. S. performed for this paper was done before he joined

Ashvattha. The conflict of interest is managed by the Johns Hopkins University.

Acknowledgements

We would like to thank Elizabeth Smith Khoury for helpful discussions of the *in vitro* experiments. This project was funded by the Patz Distinguished Professorship Endowment from Johns Hopkins and NICHD (grant number HD076901) (RMK). We thank the Wilmer Core Grant for Vision Research, Microscope and Core Module (grant number EY001865) for access to the Sony flow cytometer. We thank Servier Medical Arts for use of their collection of images (http://smart.servier.com/) that is licensed under a Creative Common Attribution 3.0 Generic License, which were modified to make the graphical abstract.

References

1 C. L. Gooch, E. Pracht and A. R. Borenstein, The burden of neurological disease in the United States: A summary report and call to action, *Ann. Neurol.*, 2017, **81**, 479–484.
2 J. L. Cummings, T. Morstorf and K. Zhong, Alzheimer's disease drug-development pipeline: few candidates, frequent failures, *Alzheimers Res. Ther.*, 2014, **6**, 37.
3 P.-P. Liu, Y. Xie, X.-Y. Meng and J.-S. Kang, History and progress of hypotheses and clinical trials for Alzheimer's disease, *Signal Transduction Targeted Ther.*, 2019, **4**, 1–22.
4 C. Soto and S. Pritzkow, Protein misfolding, aggregation, and conformational strains in neurodegenerative diseases, *Nat. Neurosci.*, 2018, **21**, 1332–1340.
5 V. H. Perry and C. Holmes, Microglial priming in neurodegenerative disease, *Nat. Rev. Neurol.*, 2014, **10**, 217–224.
6 Y. Tang and W. Le, Differential Roles of M1 and M2 Microglia in Neurodegenerative Diseases, *Mol. Neurobiol.*, 2016, **53**, 1181–1194.
7 M. W. Salter and B. Stevens, Microglia emerge as central players in brain disease, *Nat. Med.*, 2017, **23**, 1018–1027.
8 S. Krasemann, *et al.*, The TREM2-APOE Pathway Drives the Transcriptional Phenotype of Dysfunctional Microglia in Neurodegenerative Diseases, *Immunity*, 2017, **47**, 566–581. e9.
9 Q. Zhao, *et al.*, The antidepressant-like effects of pioglitazone in a chronic mild stress mouse model are associated with PPARγ-mediated alteration of microglial activation phenotypes, *J. Neuroinflammation*, 2016, **13**, 259.
10 L. Wen, *et al.*, Polarization of Microglia to the M2 Phenotype in a Peroxisome Proliferator-Activated Receptor Gamma-Dependent Manner Attenuates Axonal Injury Induced by Traumatic Brain Injury in Mice, *J. Neurotrauma*, 2018, **35**, 2330–2340.
11 W. Cai, *et al.*, Peroxisome proliferator-activated receptor γ (PPARγ): A master gatekeeper in CNS injury and repair, *Prog. Neurobiol.*, 2018, **163–164**, 27–58.
12 B. Brakedal, *et al.*, Glitazone use associated with reduced risk of Parkinson's disease, *Mov. Disord.*, 2017, **32**, 1594–1599.
13 G. M. Jojo and G. Kuppusamy, Scope of new formulation approaches in the repurposing of pioglitazone for the management of Alzheimer's disease, *J. Clin. Pharm. Ther.*, 2019, **44**, 337–348.
14 S. Mandrekar-Colucci, J. C. Karlo and G. E. Landreth, Mechanisms Underlying the Rapid Peroxisome Proliferator-Activated Receptor-γ-Mediated Amyloid Clearance and Reversal of Cognitive Deficits in a Murine Model of Alzheimer's Disease, *J. Neurosci.*, 2012, **32**, 10117–10128.
15 W. M. Pardridge, Drug transport across the blood–brain barrier, *J. Cereb. Blood Flow Metab.*, 2012, **32**, 1959–1972.
16 J. Xu, P. D. Storer, J. A. Chavis, M. K. Racke and P. D. Drew, Agonists for the peroxisome proliferator-activated receptor-α and the retinoid X receptor inhibit inflammatory responses of microglia, *J. Neurosci. Res.*, 2005, **81**, 403–411.
17 M. D. Sweeney, A. P. Sagare and B. V. Zlokovic, Blood–brain barrier breakdown in Alzheimer disease and other neurodegenerative disorders, *Nat. Rev. Neurol.*, 2018, **14**, 133–150.
18 E. S. Smith, J. E. Porterfield and R. M. Kannan, Leveraging the interplay of nanotechnology and neuroscience: Designing new avenues for treating central nervous system disorders, *Adv. Drug Delivery Rev.*, 2019, **148**, 181–203.
19 S. Kannan, *et al.*, Dendrimer-Based Postnatal Therapy for Neuroinflammation and Cerebral Palsy in a Rabbit Model, *Sci. Transl. Med.*, 2012, **4**, 130ra46–130ra46.
20 F. Zhang, *et al.*, Uniform brain tumor distribution and tumor associated macrophage targeting of systemically administered dendrimers, *Biomaterials*, 2015, **52**, 507–516.
21 D. F. Niño, *et al.*, Cognitive impairments induced by necrotizing enterocolitis can be prevented by inhibiting microglial activation in mouse brain, *Sci. Transl. Med.*, 2018, **10**, eaan0237.
22 I. Burd, *et al.*, Fetal uptake of intra-amniotically delivered dendrimers in a mouse model of intrauterine inflammation and preterm birth, *Nanomedicine*, 2014, **10**, 1343–1351.
23 Y. Guo, *et al.*, Dendrimers Target the Ischemic Lesion in Rodent and Primate Models of Nonarteritic Anterior Ischemic Optic Neuropathy, *PLoS One*, 2016, **11**, e0154437.
24 M. K. Mishra, *et al.*, Dendrimer brain uptake and targeted therapy for brain injury in a large animal model of hypothermic circulatory arrest, *ACS Nano*, 2014, **8**, 2134–2147.
25 J. C. Grimm, *et al.*, Nanotechnology Approaches to Targeting Inflammation and Excitotoxicity in a Canine Model of Hypothermic Circulatory Arrest–Induced Brain Injury, *Ann. Thorac. Surg.*, 2016, **102**, 743–750.
26 R. Sharma, *et al.*, Activated Microglia Targeting Dendrimer–Minocycline Conjugate as Therapeutics for Neuroinflammation, *Bioconjugate Chem.*, 2017, **28**, 2874–2886.
27 A. Sharma, *et al.*, Targeting Mitochondrial Dysfunction and Oxidative Stress in Activated Microglia using Dendrimer-Based Therapeutics, *Theranostics*, 2018, **8**, 5529–5547.
28 K. Liaw, *et al.*, Dendrimer size effects on the selective brain tumor targeting in orthotopic tumor models upon systemic administration, *Bioeng. Transl. Med.*, 2020, **5**, e10160.

29 E. Nance, *et al.*, Dendrimer-mediated delivery of N-acetyl cysteine to microglia in a mouse model of Rett syndrome, *J. Neuroinflammation*, 2017, **14**, 252.
30 E. Nance, *et al.*, Nanoscale effects in dendrimer-mediated targeting of neuroinflammation, *Biomaterials*, 2016, **101**, 96–107.
31 S. S. Minami, *et al.*, Selective targeting of microglia by quantum dots, *J. Neuroinflammation*, 2012, **9**, 22.
32 S. Papa, *et al.*, Selective Nanovector Mediated Treatment of Activated Proinflammatory Microglia/Macrophages in Spinal Cord Injury, *ACS Nano*, 2013, **7**, 9881–9895.
33 S. R. Cerqueira, *et al.*, Microglia response and in vivo therapeutic potential of methylprednisolone-loaded dendrimer nanoparticles in spinal cord injury, *Small Weinh. Bergstr. Ger.*, 2013, **9**, 738–749.
34 M. Esteves, *et al.*, Retinoic acid-loaded polymeric nanoparticles induce neuroprotection in a mouse model for Parkinson's disease, *Front. Aging Neurosci.*, 2015, **7**, 20.
35 A. Sharma, *et al.*, Dense hydroxyl polyethylene glycol dendrimer targets activated glia in multiple CNS disorders, *Sci. Adv.*, 2020, **6**, eaay8514.
36 R. Sharma, *et al.*, Scalable synthesis and validation of PAMAM dendrimer–N–acetyl cysteine conjugate for potential translation, *Bioeng. Transl. Med.*, 2018, **3**, 87–101.
37 M. A. Dobrovolskaia, Dendrimers Effects on the Immune System: Insights into Toxicity and Therapeutic Utility, *Curr. Pharm. Des.*, 2017, **23**, 3134–3141.
38 R. V. de Araújo, S. da S. Santos, E. Igne Ferreira and J. Giarolla, New Advances in General Biomedical Applications of PAMAM Dendrimers, *Molecules*, 2018, **23**, 2849.
39 R. E. Ratner, S. Parikh and C. Tou, Efficacy, safety and tolerability of tesaglitazar when added to the therapeutic regimen of poorly controlled insulin-treated patients with type 2 diabetes, *Diabetes Vasc. Dis. Res.*, 2007, **4**, 214–221.
40 H. Bays, J. McElhattan and B. S. Bryzinski, A double-blind, randomised trial of tesaglitazar versus pioglitazone in patients with type 2 diabetes mellitus, *Diabetes Vasc. Dis. Res.*, 2007, **4**, 181–193.
41 B. Fagerberg, *et al.*, Improvement of postprandial lipid handling and glucose tolerance in a non-diabetic population by the dual PPARα/γ agonist, tesaglitazar, *Diabetes Vasc. Dis. Res.*, 2007, **4**, 174–180.
42 B. J. Goldstein, J. Rosenstock, D. Anzalone, C. Tou and K. P. Öhman, Effect of tesaglitazar, a dual PPARα/γ agonist, on glucose and lipid abnormalities in patients with type 2 diabetes: a 12–week dose-ranging trial, *Curr. Med. Res. Opin.*, 2006, **22**, 2575–2590.
43 A. M. Lincoff, *et al.*, Effect of Aleglitazar on Cardiovascular Outcomes After Acute Coronary Syndrome in Patients With Type 2 Diabetes Mellitus: The AleCardio Randomized Clinical Trial, *J. Am. Med. Assoc.*, 2014, **311**, 1515–1525.
44 B. Ljung, *et al.*, AZ 242, a novel PPARα/γ agonist with beneficial effects on insulin resistance and carbohydrate and lipid metabolism in ob/ob mice and obese Zucker rats, *J. Lipid Res.*, 2002, **43**, 1855–1863.
45 J. Song and B.-K. Cho, Divergent Synthesis of Hydrophilic Dendrons Based on Tri(ethylene glycol) Spacers, *Bull. Korean Chem. Soc.*, 2010, **31**, 1835–1836.
46 A. Sharma, *et al.*, Effect of mannose targeting of hydroxyl PAMAM dendrimers on cellular and organ biodistribution in a neonatal brain injury model, *J. Controlled Release*, 2018, **283**, 175–189.
47 S. E. Hickman, E. K. Allison and J. E. Khoury, Microglial Dysfunction and Defective β-Amyloid Clearance Pathways in Aging Alzheimer's Disease Mice, *J. Neurosci.*, 2008, **28**, 8354–8360.
48 H. C. Kolb, M. G. Finn and K. B. Sharpless, Click Chemistry: Diverse Chemical Function from a Few Good Reactions, *Angew. Chem., Int. Ed.*, 2001, **40**, 2004–2021.
49 Tesaglitazar. https://www.drugbank.ca/drugs/DB06536.
50 D. Reker, *et al.*, "Inactive" ingredients in oral medications, *Sci. Transl. Med.*, 2019, **11**, eaau6753.
51 O. P. Perumal, R. Inapagolla, S. Kannan and R. M. Kannan, The effect of surface functionality on cellular trafficking of dendrimers, *Biomaterials*, 2008, **29**, 3469–3476.
52 R. Sharma, *et al.*, Dendrimer mediated targeted delivery of sinomenine for the treatment of acute neuroinflammation in traumatic brain injury, *J. Controlled Release*, 2020, **323**, 361–375.
53 J. E. DiCiccio and B. E. Steinberg, Lysosomal pH and analysis of the counter ion pathways that support acidification, *J. Gen. Physiol.*, 2011, **137**, 385–390.
54 S. Shibko and A. L. Tappel, Distribution of esterases in rat liver, *Arch. Biochem. Biophys.*, 1964, **106**, 259–266.
55 E. Blasi, R. Barluzzi, V. Bocchini, R. Mazzolla and F. Bistoni, Immortalization of murine microglial cells by a v-raf/v-myc carrying retrovirus, *J. Neuroimmunol.*, 1990, **27**, 229–237.
56 A. Henn, *et al.*, The suitability of BV2 cells as alternative model system for primary microglia cultures or for animal experiments examining brain inflammation, *ALTEX*, 2009, **26**, 83–94.
57 C. Ising and M. T. Heneka, Functional and structural damage of neurons by innate immune mechanisms during neurodegeneration, *Cell Death Dis.*, 2018, **9**, 120.
58 S. R. Subramaniam and H. J. Federoff, Targeting Microglial Activation States as a Therapeutic Avenue in Parkinson's Disease, *Front. Aging Neurosci.*, 2017, **9**, 176.
59 M. Rath, I. Müller, P. Kropf, E. I. Closs and M. Munder, Metabolism via Arginase or Nitric Oxide Synthase: Two Competing Arginine Pathways in Macrophages, *Front. Immunol.*, 2014, **5**, 532.
60 A. Bernardo, G. Levi and L. Minghetti, Role of the peroxisome proliferator–activated receptor–γ (PPAR–γ) and its natural ligand 15–deoxy–Δ12,14–prostaglandin J2 in the regulation of microglial functions, *Eur. J. Neurosci.*, 2000, **12**, 2215–2223.
61 S. David and A. Kroner, Repertoire of microglial and macrophage responses after spinal cord injury, *Nat. Rev. Neurosci.*, 2011, **12**, 388–399.
62 R. Vinoth Kumar, T. W. Oh and Y.-K. Park, Anti-Inflammatory Effects of Ginsenoside-Rh2 Inhibits

LPS-Induced Activation of Microglia and Overproduction of Inflammatory Mediators Via Modulation of TGF-β1/Smad Pathway, *Neurochem. Res.*, 2016, **41**, 951–957.
63 J. D. Cherry, J. A. Olschowka and M. K. O'Banion, Neuroinflammation and M2 microglia: the good, the bad, and the inflamed, *J. Neuroinflammation*, 2014, **11**, 98.
64 P. J. Murray, Macrophage Polarization, *Annu. Rev. Physiol.*, 2017, **79**, 541–566.
65 F. O. Martinez and S. Gordon, The M1 and M2 paradigm of macrophage activation: time for reassessment, *F1000Prime Rep.*, 2014, **6**, 13.
66 D. M. Mosser and J. P. Edwards, Exploring the full spectrum of macrophage activation, *Nat. Rev. Immunol.*, 2008, **8**, 958–969.
67 M. L. Dubbelaar, L. Kracht, B. J. L. Eggen and E. W. G. M. Boddeke, The Kaleidoscope of Microglial Phenotypes, *Front. Immunol.*, 2018, **9**, 1753.
68 A. Chawla, Control of macrophage activation and function by PPARs, *Circ. Res.*, 2010, **106**, 1559–1569.
69 S. M. McCormick and N. M. Heller, Regulation of Macrophage, Dendritic Cell, and Microglial Phenotype and Function by the SOCS Proteins, *Front. Immunol.*, 2015, **6**, 549.
70 C. Vaure and Y. Liu, A Comparative Review of Toll-Like Receptor 4 Expression and Functionality in Different Animal Species, *Front. Immunol.*, 2014, **5**, 316.
71 S. K. Sharma, *et al.*, Insulin-degrading enzyme prevents α-synuclein fibril formation in a nonproteolytical manner, *Sci. Rep.*, 2015, **5**, 12531.
72 J. Y. Sung, *et al.*, Proteolytic Cleavage of Extracellular Secreted α-Synuclein via Matrix Metalloproteinases, *J. Biol. Chem.*, 2005, **280**, 25216–25224.
73 M. Yamanaka, *et al.*, PPARγ/RXRα-induced and CD36-mediated microglial amyloid-β phagocytosis results in cognitive improvement in amyloid precursor protein/presenilin 1 mice, *J. Neurosci.*, 2012, **32**, 17321–17331.
74 M. A. Leissring, *et al.*, Enhanced proteolysis of beta-amyloid in APP transgenic mice prevents plaque formation, secondary pathology, and premature death, *Neuron*, 2003, **40**, 1087–1093.
75 R. E. Tanzi and L. Bertram, Twenty Years of the Alzheimer's Disease Amyloid Hypothesis: A Genetic Perspective, *Cell*, 2005, **120**, 545–555.
76 K. Liaw, O. Gök, L. B. DeRidder, S. Kannan and R. M. Kannan, Quantitative assessment of surface functionality effects on microglial uptake and retention of PAMAM dendrimers, *J. Nanopart. Res.*, 2018, **20**, 111.
77 T. V. Petrova, K. T. Akama and L. J. Van Eldik, Cyclopentenone prostaglandins suppress activation of microglia: down-regulation of inducible nitric-oxide synthase by 15-deoxy-Delta12,14-prostaglandin J2, *Proc. Natl. Acad. Sci. U. S. A.*, 1999, **96**, 4668–4673.
78 NINDS Exploratory Trials in Parkinson Disease (NET-PD) FS-ZONE Investigators, Pioglitazone in early Parkinson's disease: a phase 2, multicentre, double-blind, randomised trial, *Lancet Neurol.*, 2015, **14**, 795–803.
79 L. Dupuis, *et al.*, A Randomized, Double Blind, Placebo-Controlled Trial of Pioglitazone in Combination with Riluzole in Amyotrophic Lateral Sclerosis, *PLoS One*, 2012, **7**, e37885.
80 V. Osinski, *et al.*, In vivo liposomal delivery of PPARα/γ dual agonist tesaglitazar in a model of obesity enriches macrophage targeting and limits liver and kidney drug effects, *Theranostics*, 2020, **10**, 585–601.
81 S. Nakashiro, *et al.*, Pioglitazone-Incorporated Nanoparticles Prevent Plaque Destabilization and Rupture by Regulating Monocyte/Macrophage Differentiation in ApoE-/- Mice, *Arterioscler. Thromb. Vasc. Biol.*, 2016, **36**, 491–500.
82 D. Di Mascolo, *et al.*, Rosiglitazone-loaded nanospheres for modulating macrophage-specific inflammation in obesity, *J. Controlled Release*, 2013, **170**, 460–468.